Functional, structural and phylogenetic analysis of domains underlying the Al sensitivity of the aluminum-activated malate/anion transporter, TaALMT1

Ayalew Ligaba, Ingo Dreyer, Armine Margaryan, David J. Schneider, Leon Kochian and Miguel Piñeros

SUMMARY

Triticum aestivum **aluminum-activated malate transporter (TaALMT1) is the founding member of a unique gene family of anion transporters (ALMTs) that mediate the efflux of organic acids. A small sub-group of root-localized ALMTs, including TaALMT1, is physiologically associated with *in planta* aluminum (Al) resistance. TaALMT1 exhibits significant enhancement of transport activity in response to extracellular Al. In this study, we integrated structure–function analyses of structurally altered TaALMT1 proteins expressed in *Xenopus* oocytes with phylogenic analyses of the ALMT family. Our aim is to re-examine the role of protein domains in terms of their potential involvement in the Al-dependent enhancement (i.e. Al-responsiveness) of TaALMT1 transport activity, as well as the roles of all its 43 negatively charged amino acid residues. Our results indicate that the N-domain, which is predicted to form the conductive pathway, mediates ion transport even in the absence of the C-domain. However, segments in both domains are involved in Al^{3+} sensing. We identified two regions, one at the N-terminus and a hydrophobic region at the C-terminus, that jointly contribute to the Al-response phenotype. Interestingly, the characteristic motif at the N-terminus appears to be specific for Al-responsive ALMTs. Our study highlights the need to include a comprehensive phylogenetic analysis when drawing inferences from structure–function analyses, as a significant proportion of the functional changes observed for TaALMT1 are most likely the result of alterations in the overall structural integrity of ALMT family proteins rather than modifications of specific sites involved in Al^{3+} sensing.**

Keywords: wheat, aluminum tolerance, TaALMT1, anion channel, organic acid anion, *Xenopus laevis*, electrophysiology, *Triticum aestivum*.

INTRODUCTION

Aluminum toxicity in acid soils affects over 50% of potentially arable lands worldwide, and is the primary factor limiting agricultural productivity on these acid soils (von Uexkull and Mutert, 1995). Speciation of aluminum at low pH results in an increase in the phytotoxic form, Al^{3+}, which inhibits root growth and damages the root system, restricting water and nutrient uptake. A widespread and commonly documented Al-resistance strategy relies on exclusion mechanisms based on release of chelating ligands from the root tip, resulting in formation of non-toxic Al^{3+} complexes in the rhizosphere, which prevents the Al^{3+} from entering the root (Ma *et al.*, 2001; Kochian *et al.*, 2004). Membrane transporters from two families, the aluminum-activated malate transporter (ALMT) and multi-drug and toxin compounds extrusion (MATE) families, have been identified as the cellular mechanism(s) underlying this Al exclusion mechanism based on organic acid release (Ryan *et al.*, 2011). Membrane transporters from various families have also recently been implicated in mediating mechanisms of Al tolerance other

than those based on organic acid release (Larsen *et al.*, 2005, 2007; Huang *et al.*, 2009, 2012; Xia *et al.*, 2010; Negishi *et al.*, 2012, 2013).

Sasaki *et al.* (2004) identified and characterized the first ALMT (TaALMT1), which is the founding member of the ALMT gene family whose members encode anion transporters unique to the plant kingdom (i.e. the Viridiplantae clade), comprising seven distinct clades (Dreyer *et al.*, 2012). Within clade 1, a small sub-group of ALMTs (wheat TaALMT1, Arabidopsis AtALMT1 and *Brassica napus* BnALMT1) that are physiologically associated with *in planta* Al-tolerance responses exhibit significantly enhanced transport in the presence of extracellular Al^{3+}. Reverse genetic and physiological approaches indicate that these three ALMTs mediate root malate efflux, with the magnitude of the efflux being significantly enhanced in the presence of Al^{3+}. This results in increased levels of the Al^{3+}-chelating ligand in the rhizosphere, resulting in enhanced Al resistance (Delhaize *et al.*, 2004; Sasaki *et al.*, 2004; Pereira *et al.*, 2010; Ryan *et al.*, 2011). Heterologous expression of members of the ALMT family indicates that this Al response characteristic is intrinsic to the TaALMT sub-group (Sasaki *et al.*, 2004; Hoekenga *et al.*, 2006; Ligaba *et al.*, 2006; Piñeros *et al.*, 2008b; Zhang *et al.*, 2008). Although TaALMT1, AtALMT1 and BnALMT1 are functionally active in the absence of extracellular Al^{3+}, the unique functional property of Al-mediated enhancement of malate transport, generally referred to as Al activation, gives rise to the existing nomenclature (i.e. ALMT: Al-activated malate transport) for this entire family of transporters. However, to date, 'Al activation' has only been reported for the three ALMTs discussed above, together with modest Al activation reported for HvALMT1 from barley (Gruber *et al.*, 2010). An increasing number of reports indicate that the *in planta* roles of ALMTs extend beyond Al resistance, and include mineral nutrition, ion homeostasis, turgor regulation and guard cell function (Kovermann *et al.*, 2007; Piñeros *et al.*, 2008a; Gruber *et al.*, 2010; Meyer *et al.*, 2010a,b; Meyer *et al.*, 2011; Ligaba *et al.*, 2012; De Angeli *et al.*, 2013; Liang *et al.*, 2013). However, these ALMT transporters all lack the significant Al responsiveness reported for the TaALMT1 sub-group.

Although the increasing number of reports describing functional characterization of diverse ALMTs have clearly established that these transporters mediate organic and inorganic anion fluxes across the plasma membrane and tonoplast of cells from various tissues, our understanding of the nature of the Al^{3+}-dependent enhancement of TaALMT1 transport activity is still quite limited. The current lack of a crystal structure suitable for modeling the structure of ALMT transporters has hindered understanding of the structure–function relationships underlying ALMT-mediated transport processes, making structural and topological analysis of this transporter family challenging and controversial. Analysis based on amino acid sequences indicates that, as a family, ALMTs share a high degree of secondary structural similarity, with an N-terminus region containing six transmembrane domains, followed by a long highly hydrophilic C-terminus comprising up to half of the length of the entire protein. Functional studies on endogenous as well as heterologously expressed Al-responsive ALMTs indicate that the Al response occurs within 3–5 min, with high affinity and Al specificity, most likely involving direct interaction of Al^{3+} with the transporter (Ryan *et al.*, 1997, Piñeros and Kochian 2001, Sasaki *et al.*, 2004; Piñeros *et al.*, 2008b; Zhang *et al.*, 2008). These observations prompted investigations of negatively charged residues in TaALMT1 for their potential involvement in the molecular mechanism(s) underlying Al-dependent transport enhancement. Furuichi *et al.* (2010) examined functional changes in TaALMT1 transport activity upon neutralization of 15 negatively charged residues contained in the C-terminal domain of TaALMT1. They identified three main residues (Glu274, Asp275 and Glu284), which, upon neutralization, eliminated Al-dependent transport enhancement without affecting the basal transport activity. Based on these results and the proposed TaALMT1 topology deduced from an immunocytochemical study (Motoda *et al.*, 2007), the authors concluded that these residues, which are presumably located in an extracellularly oriented hydrophilic C-terminal region, were the key determinants of the Al-activation response. However, more recent studies have questioned this proposed topology for ALMT transporters (compare Motoda *et al.*, 2007 and Ryan *et al.*, 2011 with Meyer *et al.*, 2010a,b; Dreyer *et al.*, 2012 and Mumm *et al.*, 2013), suggesting that the C-terminal half is, at least in part, oriented towards the intracellular space, and is thus incapable of direct interaction with extracellular Al^{3+}. In addition, a recent comprehensive phylogenetic analysis showed that these three residues are highly conserved throughout the entire ALMT family, to such an extent that residue Glu284 is part of the characteristic WEP fingerprint motif (Trp-Glu-Pro) present in all ALMTs (Dreyer *et al.*, 2012). The high degree of conservation of these residues strongly indicates their importance for structural integrity, raising questions regarding their specific involvement in directly sensing Al^{3+}. Thus, are the functional changes brought upon by neutralization of these acidic residues by site-directed mutagenesis truly the result of disruption of Al^{3+} binding to the protein, or are they merely side-effects of large-scale changes to the as-yet uncharacterized tertiary structure shared by all members of the ALMT family?

In the present study, we have performed structure–function studies cross-referenced to phylogenetic analyses in order to identify potential protein domains underlying functional characteristics of TaALMT1, particularly the Al-dependent enhancement of its transport activity. In light

of the recent controversy over ALMT topology, our study evaluates structural changes throughout the protein without making *a priori* assumptions regarding the orientation of the protein. Integration of our structure–function findings with phylogenetic analyses allowed us to re-assess the role of protein domains and negatively charged residues in terms of overall conservation and structural integrity, as well as their potential role in the molecular mechanism leading to the Al-dependent response. Our data indicate that the N-domain, which is predicted to form the conductive pathway, can mediate organic anion transport in the absence of the C-domain. However, regions in both the N- and C-domains are involved in Al-mediated enhancement of transport activity. Most notably, we have identified a characteristic motif at the extreme N-terminus of Al-responsive ALMTs that is correlated with the Al-response phenotype.

RESULTS AND DISCUSSION

Removal of the entire C-domain does not affect TaALMT1 basal transport activity but abolishes Al responsiveness

Initially, we generated a series of sequential deletions at the C-terminus of TaALMT1. The first two deletions examined comprised removal of the entire C-domain at a highly conserved region after the last transmembrane region present in the N-domain (TaALMT1$^{\Delta 219\ 459}$ in Figure 1). In the absence of extracellular Al^{3+}, oocytes expressing TaALMT1$^{\Delta 219\ 459}$ mediated inward currents of similar magnitude (-233 ± 9 nA at -140 mV) to those recorded for the full TaALMT1 protein (-222 ± 10 nA). However, while the inward currents for the full-length TaALMT1 were significantly enhanced by extracellular Al^{3+} (i.e. were Al-responsive) as described previously (Piñeros *et al.*, 2008b; Furuichi *et al.*, 2010), the transport activity of TaALMT1$^{\Delta 219\ 459}$ was insensitive to Al^{3+}. This result was puzzling, as Furuichi *et al.* (2010) had reported that, under identical ionic conditions, a similar truncation (TaALMT1$^{\Delta 221\ 459}$), differing only by two amino acids, was not functionally expressed in oocytes, suggesting that the C-domain was critical for both basal transport as well as Al-enhanced activity. To address this experimental contradiction, we generated and tested the transport activity of TaALMT1$^{\Delta 221\ 459}$ studied by Furuichi *et al.* (2010). As shown in Figure 1(b–d), TaALMT1$^{\Delta 221\ 459}$ may be expressed in a functional form in oocytes, where it mediates a basal malate transport activity (approximately -200 nA at -140 mV) that is comparable to that recorded for TaALMT1$^{\Delta 219\ 459}$ and full-length TaALMT1. As for TaALMT1$^{\Delta 219\ 459}$, TaALMT1$^{\Delta 221\ 459}$ transport activity was also insensitive to extracellular Al^{3+}, indicating that, in contrast to the previous report (Furuichi *et al.*, 2010), the C-terminal domain is not required for basal transport but is essential for maintaining Al responsiveness. Expression and localization of the chimeric EGFP::TaALMT1$^{\Delta 219\ 459}$ and EYFP::TaALMT1$^{\Delta 219\ 459}$ proteins in both *Xenopus* oocytes and Arabidopsis protoplasts indicated that the truncated protein is localized to the plasma membrane (Figure 1d–g), as has been shown for the native TaALMT1 protein (Yamaguchi *et al.*, 2005). These findings also demonstrate that the N-domain of the TaALMT1 protein, consisting primarily of the highly conserved hydrophobic region of ALMTs spanning six predicted transmembrane domains, may be functionally expressed and constitutes the conductive pathway even in the absence of the C-domain (Figure 1). However, although the N-domain is functionally active, lack of the C-domain of TaALMT1 resulted in loss of Al responsiveness.

The enhancement of the full-length TaALMT1 transport by extracellular Al^{3+} may be considered analogous to processes described for ligand-gated channels, for which changes in channel gating by intracellular ligands depend on certain motifs constituting binding and gating sites. The binding sites allow the channel to be modulated by a specific ligand molecule, while the gating site controls the channel activity. For example, the large-conductance calcium-activated potassium channel (BK_{Ca}), which in animal cells is activated both by voltage as well as intracellular calcium, shares a similar domain architecture to TaALMT1, consisting of an N-domain containing seven transmembrane regions followed by a long intracellular highly hydrophilic C-terminus with distinct ligand sites comprising approximately half the length of the entire protein. Removal of the entire BK_{Ca} intracellular C-terminus (believed to contain the calcium-binding site or 'calcium bowl') also resulted in functionally active channels that lack the calcium responsiveness of the native protein (Piskorowski and Aldrich, 2002). This type of finding highlights the complex coupling that may occur between ligand binding and channel gating, and the multiple ways that these processes may be coupled. By analogy, our findings suggest that either the TaALMT1 C-domain contains the required high-affinity Al-binding sites and/or residues present in the C-domain interact with regions in the N-domain to modify TaALMT1 gating characteristics upon binding Al.

Truncations within the C-domain reveal domains essential for TaALMT1 function and Al sensitivity

The above results suggest that the C-domain contains motifs required for the Al^{3+} responsiveness of N-domain-mediated transport. We therefore generated a series of smaller C-domain truncations, some of which also include the putative phosphorylation sites that we identified previously (Ligaba *et al.*, 2009). Unexpectedly, expression of the TaALMT1$^{\Delta 329\ 459}$ truncation, which contains approximately 50% of the C-domain, including the first putative phosphorylation site, resulted in a sig-

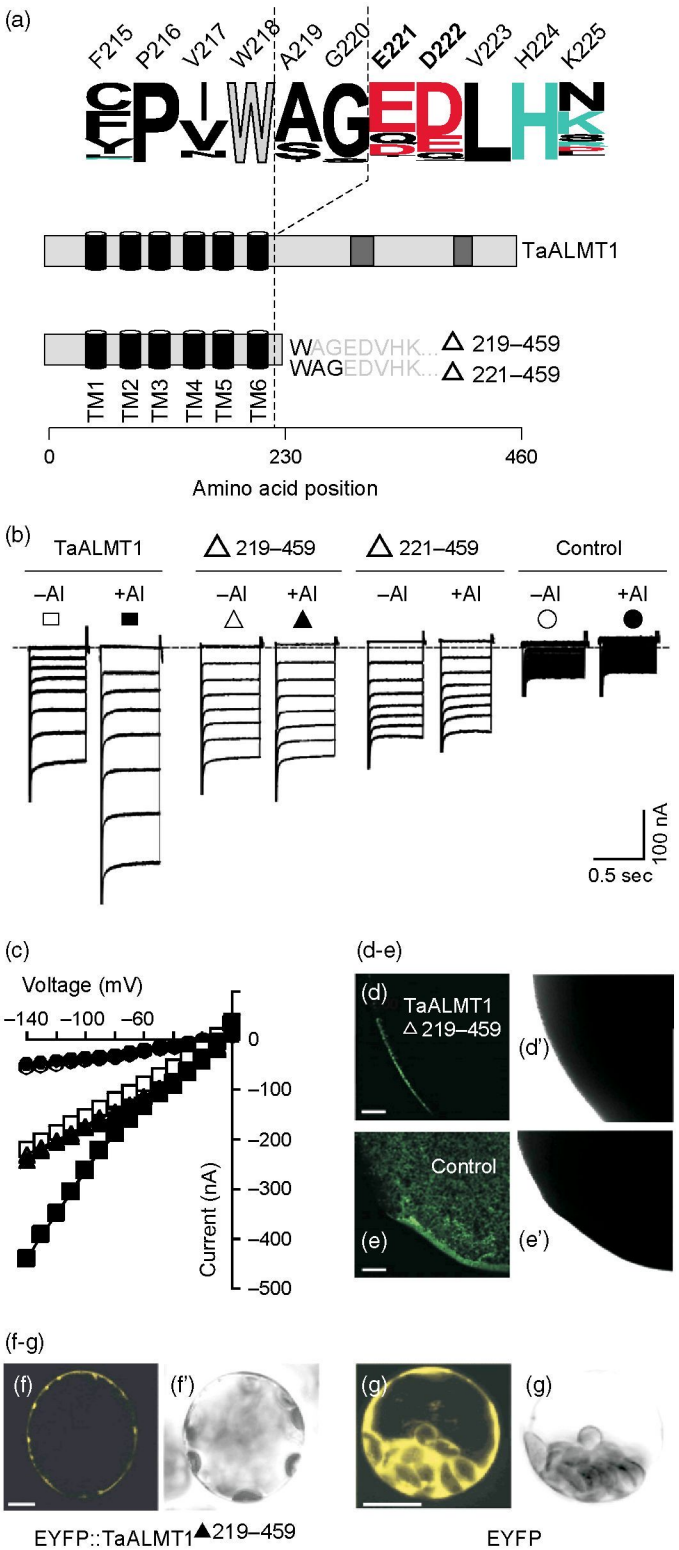

Figure 1. Expression of the N-terminal half of TaALMT1 in oocytes translates into a functional transport protein.

(a) Diagram illustrating the conserved secondary structure of ALMT transporters. Top row: sequence logo illustrating the degree of conservation of the regions flanking residues 218–220. For generation of the logo, 386 ALMT sequences from all five clades were used (122 from clade 1; 99 from clade 2; 83 from clade 3; 60 from clade 4; 22 from clade 5). Middle row: the full-length TaALMT1 consists of six transmembrane domains contained in the first half (i.e. the N-terminus) of the protein, with the remaining half (i.e. the C-terminus) consisting of a highly hydrophilic region. The darker gray boxes in the C-terminus illustrate the positions of two putative hydrophobic regions (Dreyer *et al.*, 2012). No *a priori* assumptions have been made regarding the extracellular or intracellular orientation of the N- and C-terminal regions. Bottom row: diagram illustrating the resulting truncated proteins upon removal of the C-terminal region. The region (i.e. amino acid sequence) of the C-terminal deletions is indicated by Δ followed by the amino acid positions relative to native TaALMT1, with the site of the truncation indicated by the gray amino acid sequence.

(b) Representative current traces recorded in cells expressing two C-terminal truncations (TaALMT1$^{\Delta 219-459}$ and TaALMT1$^{\Delta 221-459}$), relative to those measured in cells expressing full-length TaALMT1. Currents from control cells (i.e. not injected with cRNA) are shown for reference. Holding potentials ranged from −140 to 0 mV (+20 mV steps) using the voltage protocol described in Experimental Procedures. Recordings were performed in ND96 (pH 4.5) with or without Al^{3+} as indicated above each set of traces. The solid horizontal line represents the zero current level.

(c) Mean current–voltage (*I*/*V*) curves constructed from steady-state current recordings such as those shown in (b). The symbols for each construct and ionic conditions used are shown above the representative traces shown in (b).

(d–g) Cellular localization of TaALMT1$^{\Delta 219-259}$. The EGFP::TaALMT1$^{\Delta 219-259}$ and EYFP::TaALMT1$^{\Delta 219-259}$ chimeras localized to the plasma membrane when expressed in oocytes (d) or Arabidopsis protoplasts (f), respectively. Controls using soluble EGFP in *Xenopus* oocytes (e) and EYFP in protoplasts (g) are shown for reference. The corresponding bright-field images are shown in (d')–(g'). Scale bars = 100 μm for oocytes and 10 μm for protoplasts.

nificant reduction in basal transport activity and loss of Al responsiveness (Figure 2a,b). In fact, TaALMT1$^{\Delta 329\ 459}$ transport activity was only slightly greater than the endogenous activity in control oocyte cells not expressing TaALMT1 (−85 ± 9 nA recorded at −140 mV compared to −55 ± 8 nA, respectively). Localization of the

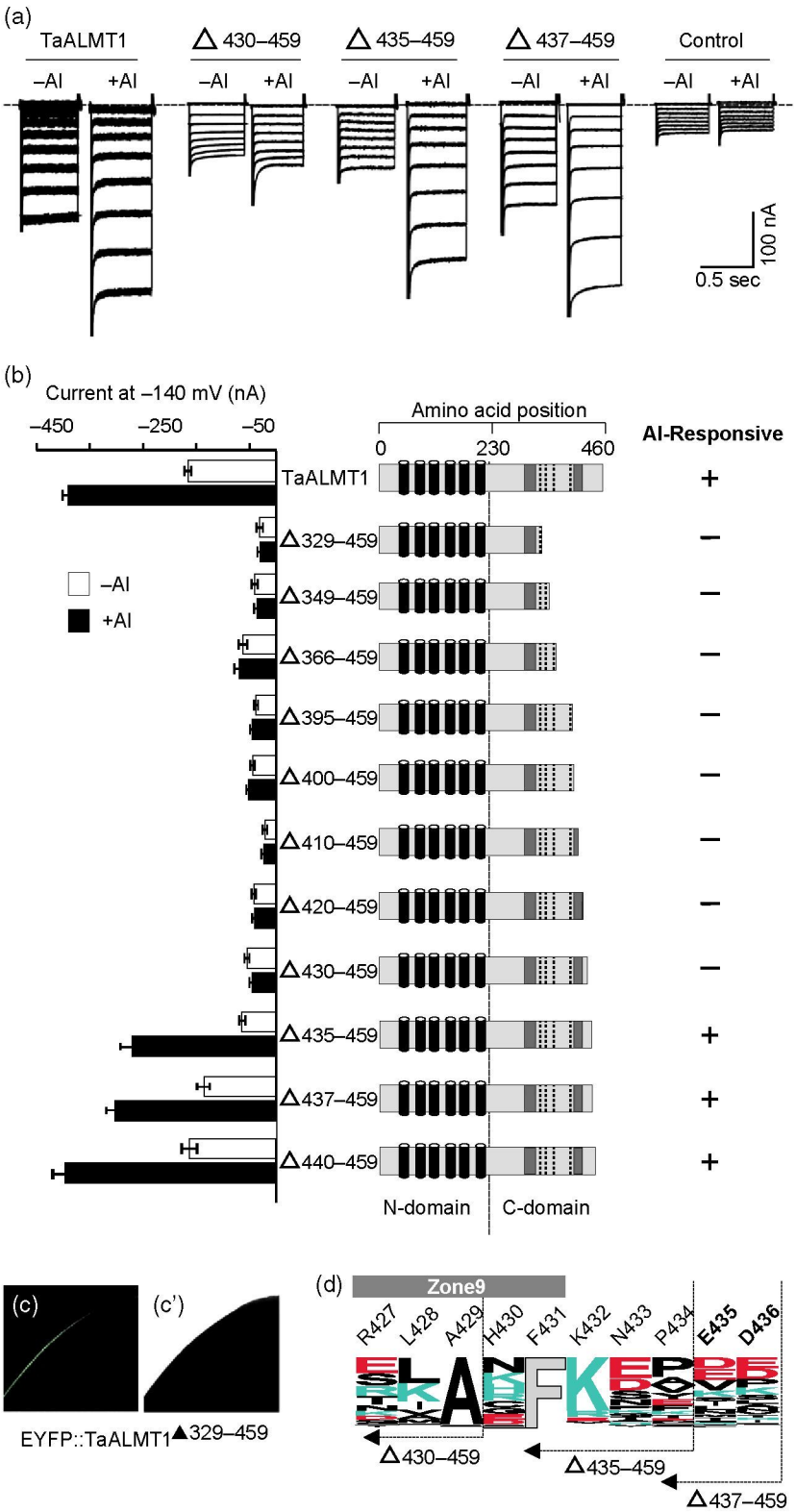

Figure 2. Truncations within the C-domain revealed regions essential for TaALMT1 function and Al responsiveness.

(a) Representative current traces measured in cells expressing three representative C-domain truncations (TaALMT1$^{\Delta 430–459}$, TaALMT1$^{\Delta 435–459}$ and TaALMT1$^{\Delta 437–459}$) recorded in the absence and presence of extracellular Al^{3+}. Current traces for the full-length TaALMT1 and control cells are shown for reference in the left and right panels, respectively. The dashed horizontal line represents the zero current level.

(b) Changes in basal transport (open bars recorded in the absence of Al^{3+}) and Al responsiveness (closed bars recorded in the presence of Al^{3+}) for a series of C-domain truncations. The histograms show the magnitude of inward currents in response to a holding potential of −140 mV recorded in cells expressing full-length TaALMT1 or the sequential C-terminal truncations in the absence or presence of Al^{3+}. The endogenous currents measured in control oocytes (i.e. not injected with cRNA) have been subtracted. The diagrams on the right indicate the position and length of each truncation relative to the full-length TaALMT1. Dotted lines in the C-domain indicate putative phosphorylation sites (S324, S337, S351 and S384). The darker gray boxes show the positions of two putative hydrophobic regions in the C-terminal domain (Dreyer *et al.*, 2012). The plus and minus symbols on the far right indicate the presence (+) or absence (−) of Al responsiveness for each truncation.

(c) Plasma membrane localization of the EGFP::TaALMT1$^{\Delta 329–459}$ chimera expressed in oocytes. The bright-field image is shown in (c'). Scale bar = 100 μm.

(d) Sequence logo illustrating the degree of conservation of the regions flanking residues 430–440. For generation of the logo, 347 sequences from all five clades were used (117 from clade 1; 92 from clade 2; 68 from clade 3; 55 from clade 4; 15 from clade 5). Zone 9, which is highly conserved among ALMTs (Dreyer *et al.*, 2012), is indicated.

EGFP::TaALMT1$^{\Delta 329\ 459}$ chimeric protein indicated that the protein was localized to the oocyte plasma membrane, suggesting that the lack of transport activity is not due to disruption of protein expression or protein targeting to the plasma membrane (Figure 2c). Expression of any of the truncated TaALMT1 proteins that included the remain-

ing three putative phosphorylation sites (TaALMT1$^{\Delta 349\ 459}$, TaALMT1$^{\Delta 366\ 459}$ and TaALMT1$^{\Delta 395\ 459}$) resulted in transporters with similarly inhibited transport activities (Figure 2b). Subsequently, smaller C-domain deletions were generated (TaALMT1$^{\Delta 400\ 459}$, TaALMT1$^{\Delta 410\ 459}$ and TaALMT1$^{\Delta 430\ 459}$) in an attempt to establish the minimum C-domain requirement for basal TaALMT1 transport and full Al enhancement. These smaller truncations, which included up to 94% of the full-length TaALMT1, exhibited the same inhibition of transport described for the larger truncations. As deletions from the end of the C-terminus of as little as 30 residues (TaALMT1$^{\Delta 430\ 459}$) strongly reduced TaALMT1 transport activity, we examined the effect of deleting the terminal 20 residues (TaALMT1$^{\Delta 440\ 459}$) and 25 residues (TaALMT1$^{\Delta 435\ 459}$). Expression of these truncations resulted in transporters with partial (TaALMT1$^{\Delta 435\ 459}$) and full (TaALMT1$^{\Delta 440\ 459}$) basal and Al-enhanced transport activity (Figure 2b).

As negatively charged residues have been implicated in the potential Al^{3+} binding and subsequent activation of the transporter (Furuichi *et al.*, 2010), we investigated the potential role of E435 and D436 by examining the activity of a TaALMT1$^{\Delta 437\ 459}$ truncation. Expression of TaALMT1$^{\Delta 437\ 459}$ resulted in a moderate increase in both basal and Al-enhanced transport activity relative to TaALMT1$^{\Delta 435\ 459}$ (Figure 2b). However, minor differences in expression levels between TaALMT1$^{\Delta 435\ 459}$ and TaALMT1$^{\Delta 437\ 459}$ could not be ruled out as the source of the observed differences. Nonetheless, these results indicate that the residues between His430 and Pro434 (Figure 2d) are important for the Al responsiveness of TaALMT1, while the terminal 23 amino acids do not play a significant role. Interestingly, the region including amino acids 430–436 is immediately downstream of a hydrophobic region (residues 400–432) that is conserved among ALMTs. It has been hypothesized that this region may constitute a potential transmembrane domain, or, alternatively, a region that is anchored to the membrane (zone 9, see Dreyer *et al.*, 2012). Thus, it is tempting to propose that restoration of full transport functionality and Al gating in TaALMT1$^{\Delta 435\ 459}$ results from inclusion of this conserved protein region. This domain may play a critical role in allowing the C-domain to properly interact with the other transmembrane regions and participate in channel gating/modulation. The loss of transport activity observed in TaALMT1 truncated variants smaller than TaALMT1$^{\Delta 435\ 459}$ may be the product of structural instability of an unanchored hydrophilic C-region, rather than due to disruption of any of the putative C-domain phosphorylation sites identified previously in TaALMT1 (Ligaba *et al.*, 2009). Therefore, the partial functional reconstitution (i.e. lacking Al enhancement) for the longer C-terminus truncations including TaALMT1$^{\Delta 219\ 459}$ and TaALMT1$^{\Delta 221\ 459}$ may result from the complete removal of the otherwise unstable hydrophilic C-region.

Re-evaluation of residues potentially involved in mediating Al enhancement of transport activity

In contrast to all ALMT members functionally characterized to date, only TaALMT1 and its Arabidopsis and *Brassica napus* homologs AtALMT1 and BnALMT1 (as well as HvALMT1 to a lesser degree) display the unique characteristic of enhancement of transport by the presence of extracellular Al^{3+} ($EC_{50} = 5 \pm 1\ \mu M\ Al^{3+}$), with maximum enhancement occurring within a few minutes of exposure (Hoekenga *et al.*, 2006; Piñeros *et al.*, 2008b). The high affinity and the time course of the response (3–5 min) have led researchers to propose that the enhancement may involve direct binding of Al^{3+} to the transporter. This prompted Furuichi *et al.* (2010) to evaluate the potential role of several negatively charged residues from the C-terminal half of TaALMT1 with regard to its Al responsiveness, based on the assumption that this region is located on the extracellular side of the plasma membrane, as proposed by Motoda *et al.* (2007). However, in light of the opposite orientation proposed for ALMTs by other groups (Meyer *et al.*, 2010a,b; Mumm *et al.*, 2013), and the increasing number of available sequences that allowed Dreyer *et al.* (2012) to perform a comprehensive phylogenetic analysis on the degree of conservation of some of these residues throughout the ALMT family, we re-evaluated the potential role of all of the negatively charged residues (43 in total) in TaALMT1 without making any *a priori* assumptions regarding their potential orientation/topology or degree of conservation.

Role of negatively charged residues in the C-domain. Figure 3 highlights the functional changes relative to native TaALMT1 obtained by individual neutralization of the 27 negatively charged residues present in the C-domain of TaALMT1. None of the substitutions led to complete loss of TaALMT1 transport activity. Instead, they yielded a continuous spectrum of Al-responsive transport activities (Figure 3b). Closer inspection of the data revealed four mutants (E248Q, E274Q, D275N and D423N) with extreme effects. E248Q exhibited a moderately increased Al enhancement compared with the wild-type, while the other three were totally insensitive to Al. The remarkable loss of Al response observed for E274Q and D275N (and E284Q to a lesser degree) was in agreement with the previous report by Furuichi *et al.* (2010). In contrast, the Al insensitivity of D423N (Figure 3) differs from the modest reduction reported in the previous study (Furuichi *et al.*, 2010) for the E420Q/D423N double mutant, suggesting that the Al responsiveness of the transporter may be the result not only of single-residue substitutions, but also potentially the product of allosteric interactions within a given protein region. Similarly, the observed loss of the Al response in the E274Q, D275N and D284Q mutants may be the results

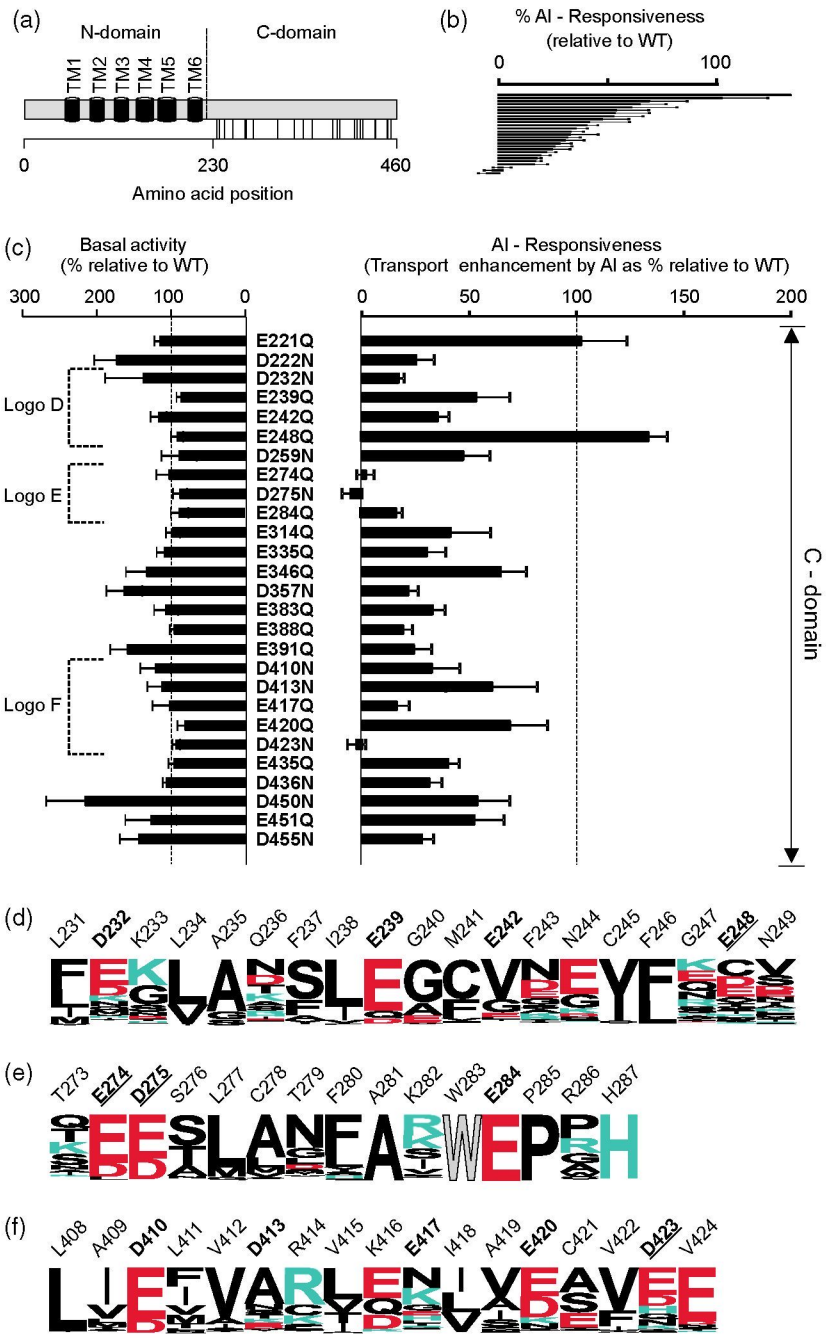

Figure 3. Mutagenesis-mediated neutralization of individual acidic residues in the C-domain resulted in transporters that vary in their degree of Al^{3+} responsiveness.

(a) Diagram illustrating the distribution of the 27 negatively charged residues (indicated by vertical lines under the diagram) throughout the C-terminus regions of the full-length TaALMT1 protein. No *a priori* assumptions have been made regarding the extracellular or intracellular orientation of the N- and C-terminal regions.

(b) Overall distribution of the changes in Al responsiveness upon neutralization of the 27 negatively charged residues in the C-terminus. The percentage Al responsiveness for a given mutant TaALMT1 is relative to the Al enhancement recorded for the full-length TaALMT1. The residues are sorted in descending order with respect to their Al response.

(c) Changes in basal (left panel) and Al^{3+}-enhanced (right panel) transport properties for the 27 residue substitutions. Values were determined by comparing the mean inward currents recorded at a holding potential of −140 mV in the absence (basal transport) and presence (Al^{3+} transport enhancement) of 100 μM $AlCl_3$, and are expressed as a percentage relative to that recorded for unmodified TaALMT1 (set to 100% as indicated by the vertical dashed line).

(d–f) Sequence logos illustrating the regions flanking residues D232, E239, E242 and E248 (d), E274, D275 and E284 (e), and D410, D413, E417, E420 and D423 (f). The transport activity of these neutralized residues is indicated in the left part of (c) by brackets labeled as 'Logo D', 'Logo E' or 'Logo F'. For generation of the logos, sequences from all five clades were used: (d) total 360; 114 from clade 1, 94 from clade 2, 80 from clade 3, 50 from clade 4, 22 from clade 5; (e) total 365; 120 from clade 1, 98 from clade 2, 75 from clade 3, 51 from clade 4, 21 from clade 5; (f) total 373; 122 from clade 1, 94 from clade 2, 81 from clade 3, 57 from clade 4, 19 from clade 5.

of structural effects rather than due to disruption of key determinants of Al sensitivity as proposed previously (Furuichi *et al.*, 2010). This hypothesis is further supported by the increasing amount of ALMT sequence data. A detailed phylogenetic analysis of ALMTs showed that there is a high degree conservation of the negatively charged residues in the C-domain throughout the entire ALMT family, with such residues being either highly conserved, or if not, at least present in both Al-sensitive and Al-insensitive ALMTs characterized to date (Figure 3 and Table 1). This observation suggests that loss of the Al-dependent response may be due to a generic loss of structural integrity, rather than confirmation of their specific involvement in Al responsiveness. Nonetheless, a few negatively charged residues (259, 346, 413, 417, 451 and 455) are unique to TaALMT1, with all of them resulting in a 50–75% loss of Al responsiveness (compared to the unmodified TaALMT1) when neutralized. Interestingly, although neutralization of residues 451 and 455 results in an approximately 25–50% reduction in Al responsiveness (Figure 3), removal

Table 1 Phylogenetic and functional features of negatively charged residues in the C-domain of TaALMT1

Residue	Features	Al responsiveness
E221	Conserved in ALMTs of all clades	+
D222	Conserved in ALMTs of all clades	– –
D232	Conserved in ALMTs of clades 1 and 3	– –
E239	Conserved in ALMTs of all clades	+
E242	Present in Al-sensitive and Al-insensitive ALMTs	–
E248	Present in Al-sensitive and Al-insensitive ALMTs	+
D259	Unique to TaALMT1	–
E274	**Highly conserved in ALMTs of all clades**	– – –
D275	**Highly conserved in ALMTs of all clades**	– – –
E284	Highly conserved in ALMTs of all clades	– –
E314	Conserved in ALMTs of clades 1 and 4	–
E335	Conserved in ALMTs of clades 1 and 2	–
E346	Unique to TaALMT1	+
D357	Conserved in ALMTs of clades 1, 2 and 3	– –
E383	Not conserved, present in Al-sensitive and Al-insensitive ALMTs	–
E388	Not conserved, present in Al-sensitive and Al-insensitive ALMTs	– –
E391	Not conserved, present in Al-sensitive and Al-insensitive ALMTs	– –
D410	Highly conserved in ALMTs of all clades	–
D413	Unique to TaALMT1	+
E417	Unique to TaALMT1	– –
E420	Conserved in ALMTs of all clades	+
D423	**Present in ALMTs of all clades, and present in Al-sensitive and Al-insensitive ALMTs**	– – –
E435	Present in ALMTs of all clades	–
D436	Present in ALMTs of all clades	–
D450	Present in Al-sensitive and Al-insensitive ALMTs	+
E451	Unique to TaALMT1	+
D455	Unique to TaALMT1	–

Bold represents residues previously identified by Furuichi *et al.* (2010).
Levels of Al-responsiveness are relative to those observed for the unmodified TaALMT1:
(+), 50% or more of the Al responsiveness observed for the unmodified TaALMT1;
(-), 25 to 50% of the Al responsiveness observed for the unmodified TaALMT1;
(--), less than 25% of the Al responsiveness observed for the unmodified TaALMT1;
(---), total loss of Al- responsiveness.

of these residues (i.e. TaALMT1$^{\Delta 450\ 459}$ in Figure 2) resulted in a transporter with similar Al responsiveness to that observed in the unmodified TaALMT1.

As a proof of concept that structural changes in highly conserved residues can result in misleading phenotypes (i.e. loss of Al response) that mimic the changes in biophysical properties (i.e. loss of Al sensitivity) described for the highly conserved negative residues mentioned above, we evaluated the potential functional changes that occur in TaALMT1 when three highly conserved neutral residues (identified in the phylogenetic analysis: Figure 4) are independently replaced by alanine, an ambivalent non-reactive residue. Amino acid W218 follows immediately after the sixth transmembrane domain (see Figure 1a). W283 is part of the WEP motif in the C-terminal zone 3 (see Dreyer *et al.*, 2012; Figure 3e) of ALMT family proteins, and precedes E284, mutation of which resulted in significant inhibition of the Al response (Figure 3c). Finally, F431 flanks the end of the C-terminal zone 9 (Figure 2d). Inward currents recorded from cells expressing W218A or W283A were significantly smaller than those recorded for TaALMT1, and were Al-insensitive (Figure 4a), resembling those described above for TaALMT1 mutated at highly conserved negatively charged residues (Figure 3). In contrast, no significant inward currents (relative to control cells) were recorded from cells injected with F431A cRNA. Expression and localization of EGFP::TaALMT1^{W218A}, EGFP::TaALMT1^{W283A} and EGFP::TaALMT1^{F431A} in *Xenopus* oocytes indicated that the functional changes are not due to absence of protein expression or disruption of protein targeting, but rather are associated with structural changes (Figure 4b–g).

Thus, if highly conserved residues cannot be used as an indicator of the Al response, as they are most likely related to overall structural integrity/functionality, are any of the negatively charged residues unique to the C-domain of TaALMT1 (259, 346, 413, 417, 451 and 455; see Table 1) key elements determining Al responsiveness? Given the lessons learned from the misleading inferences drawn solely based on single-residue mutation analysis, we

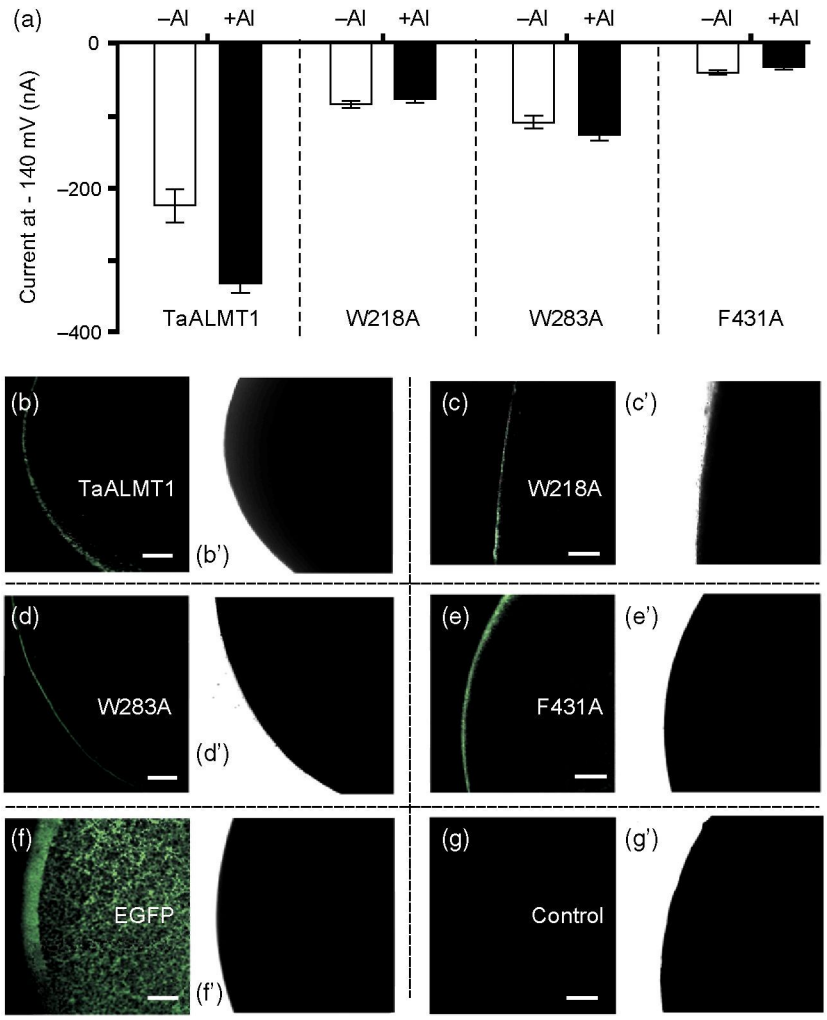

Figure 4. Single-residue mutations of highly conserved and neutral residues disrupt basal and Al^{3+}-enhanced TaALMT1-mediated transport.
(a) Mean currents measured from cells expressing full-length TaALMT1 or the mutants W218A, W284A and F431A, recorded in the present or absence of Al^{3+}. Endogenous currents measured in control cells (i.e. cells not injected with cRNA) were subtracted. The logos illustrating the degree of conservation of the W218, W284 and F431 residues are shown in Figures 1(a), 2(d) and 3(d), respectively, with the corresponding residues shown in gray.
(b–g) Cellular localization of the N-terminal EGFP chimeras for the W218A (c), W284A (d) and F431A (e) mutant proteins expressed in oocytes. Control cells expressing EGFP::TaALMT1 (b), soluble EGFP (f) or non-injected (g) are shown for reference. The corresponding bright-field images are shown in the (b')–(g'). Scale bar = 100 μm.

cannot support a key role in Al responsiveness for the C-domain or any of the identified and unique TaALMT1 residues. Instead, given the potential interactions of various regions throughout the protein, we extended the amino acid substitution analysis to include all negative residues present in the currently overlooked N-domain.

Role of negatively charged residues in the N-domain. The N-domain consists of an N-terminal region of approximately 50 residues (containing seven negatively charged residues) prior to the hydrophobic region of approximately 170 residues constituting the six putative transmembrane domains, where an additional nine negative residues are found in transmembrane regions as well as in loops with the opposite topological orientation (Figure 5a). As observed for the C-domain, individual substitution of the 16 negatively charged residues in the N-domain resulted in a continuous distribution of functional changes with respect to the Al responsiveness that appear uncorrelated with putative membrane topology (Figure 5b). None of the substitutions resulted in abolishment of basal transport activity (except E127Q in TM3, which showed a partial reduction). However, in contrast to the mutations in the C-domain, a few substitutions in the N-terminal region (D2N, E8Q, D10N and D49N) actually resulted in increased basal transport activity. Given that the increase in basal transport activity of these four substitutions was accompanied by a decrease in Al enhancement of transport, the functional changes recorded for these transporters appear to result from structural changes rather than potential variation in cRNA injection and protein expression. Furthermore, the Al responsiveness of other N-terminal mutants may also be influenced by changes in TaALMT1 structure. While E188Q showed no functional differences relative to TaALMT1, substitutions in loop regions with opposite membrane orientation (E137 in the TM3–4 loop and D166N in the TM4–5 loop) resulted in total loss of Al enhancement. Likewise, substitutions at positions predicted to be embedded within transmembrane domains (E95 and E127) also resulted in a significant reduction in Al responsiveness. To obtain insights into potential structural aspects,

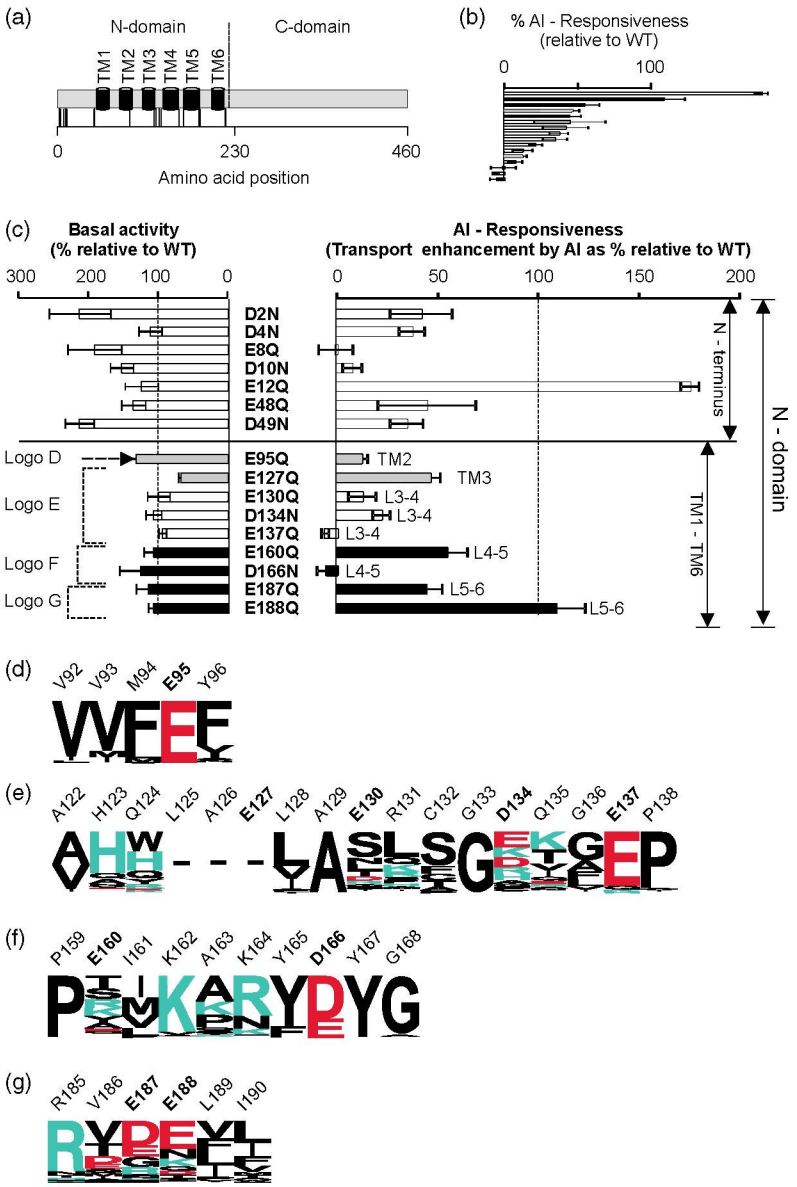

Figure 5. Mutagenesis-mediated neutralization of individual acidic residues in the N-domain resulted in transporters that vary in their degree of Al^{3+} responsiveness.

(a) Diagram illustrating the distribution of the 16 negatively charged residues (indicated by vertical lines under the diagram) throughout the N-domain region of the TaALMT1 protein.

(b) Overall distribution of the changes in Al responsiveness upon neutralization of the 16 negatively charged residues in the N-terminus. The percentage Al responsiveness for a given mutant TaALMT1 is relative to the Al enhancement recorded for the full-length TaALMT1. The residues are sorted in descending order with respect to their Al response.

(c) Changes in basal (left panel) and Al^{3+}-enhanced (right panel) transport properties for the 16 residue substitutions. Values were determined by comparing the mean inward currents recorded at a holding potential of −140 mV in the absence (basal transport) and presence (Al^{3+} transport enhancement) of Al^{3+}, and are expressed as a percentage relative to that recorded in the unmodified TaALMT1 (set to 100% as indicated by the vertical dashed line). The N-domain has been sub-divided into the most N-terminal region and the region containing the predicted TM1–6. No *a priori* assumptions have been made regarding the extracellular or intracellular orientation of the N- and C-terminal regions. White and black bars represent residues located at opposite sides of the plasma membrane (following the same convention used in Figure 3); gray bars represent predicted transmembrane domains. The notation on the right of each histogram indicates the location of the residue: TM*x* = transmembrane domain; L*x*–*y* = the loop between TM*x* and TM*y*.

(d–g) Sequence logos illustrating the regions flanking residues E95 (d), E127, E130, D134 and E137 (e), E160 and D166 (f), and E187 and E188 (g). The transport activity of these neutralized residues is indicated in the left part of (c) by brackets labeled as 'Logo D', 'Logo E', 'Logo F' and 'Logo G'. For generation of the logos shown in (d), (f) and (g), sequences from all five clades were used: (d) total 386; 128 from clade 1, 95 from clade 2, 84 from clade 3, 57 from clade 4, 22 from clade 5; (f) total 384; 126 from clade 1, 94 from clade 2, 85 from clade 3, 57 from clade 4, 22 from clade 5; (g) total 375; 127 from clade 1, 96 from clade 2, 76 from clade 3, 57 from clade 4, 19 from clade 5. The linker between TM3 and TM4 shows only similarities in ALMTs from clades 1, 4 and 5. Therefore, only sequences belonging to these three clades contributed to the logo shown in (e) (total 195; 118 from clade 1, 56 from clade 4, 21 from clade 5).

Table 2 Phylogenetic and functional features of negatively charged residues in the N-domain of TaALMT1

Residue	Features	Region	Al responsiveness
D2	Present in Al-sensitive and Al-insensitive ALMTs	N-terminal	–
D4	Part of a unique motif of positive and negative amino acids that are conserved in Al-sensitive channels but absent in Al-insensitive channels	N-terminal	–
E8	Part of a unique motif of positive and negative amino acids that are conserved in Al-sensitive channels but absent in Al-insensitive channels	N-terminal	– – –
D10	Part of a unique motif of positive and negative amino acids that are conserved in Al-sensitive channels but absent in Al-insensitive channels	N-terminal	– –
E12	Part of a unique motif of positive and negative amino acids that are conserved in Al-sensitive channels but absent in Al-insensitive channels	N-terminal	+++
E48	Highly conserved in ALMTs of clades 1, 3, 4 and 5	N-terminal	–
D49	Highly conserved in ALMTs of clades 1, 3, 4 and 5	N-terminal	–
E95	Highly conserved in ALMTs of all clades	TM1–TM6	– –
E127	Unique to TaALMT1	TM1–TM6	–
E130	Unique to TaALMT1	TM1–TM6	– –
D134	Present in the Al-sensitive TaALMT1 and the Al-insensitive ZmALMT1 and ZmALMT2	TM1–TM6	–
E137	**Highly conserved in ALMTs of clades 1, 4 and 5**	**TM1-TM6**	– – –
E160	Present in the Al-sensitive TaALMT1 and the Al-insensitive ZmALMT1 and ZmALMT2	TM1–TM6	–
D166	**Highly conserved in ALMTs of all clades**	**TM1-TM6**	– – –
E187	Present in Al-sensitive and Al-insensitive ALMTs	TM1–TM6	–
E188	Present in Al-sensitive and Al-insensitive ALMTs	TM1–TM6	+

Bold represents residues previously identified by Furuichi *et al.* (2010).
Levels of Al-responsiveness are relative to those observed for the unmodified TaALMT1:
(+), 50% or more of the Al responsiveness observed for the unmodified TaALMT1;
(-), 25 to 50% of the Al responsiveness observed for the unmodified TaALMT1;
(--), less than 25% of the Al responsiveness observed for the unmodified TaALMT1;
(---), total loss of Al- responsiveness.

we also assessed the experimental results in the light of phylogenetic analyses. Table 2 summarizes the phylogenetic characteristics/conservation of the N-domain negative residues throughout the ALMT family. Within this N-domain, with the exception of E127 and E130, all other negatively charged residues appear to be highly conserved throughout the family, making it difficult to assign them specific roles in determining Al responsiveness. As for the C-domain, it is not feasible to distinguish between generic involvements in structural integrity as opposed to a specific role in determining Al responsiveness. As with the negative residues in the C-terminus, we feel it is impossible to support a direct role for any of these N-terminus negative residues in the Al-dependent enhancement of TaALMT1 anion transport.

Our data indicate that the structural/functional relations underlying Al binding and changes in gating (e.g. stabilization of the open state) may be so complex that structural alterations may cause changes in gating without necessarily directly affecting the Al-binding site itself. Thus, a simple model based on individual mutations aimed at describing this relationship is inadequate to interpret the functional changes. Rather, the overall results suggest that Al responsiveness emerges from a collective process of interactions among a number of residues from both the N- and C-domains. In fact, changes in ion-channel gating of ligand-gated channels have been shown to involve complex interactions of multiple domains (e.g. Gordon *et al.*, 1997; Varnum and Zagotta, 1997; Gonzalez *et al.*, 2012).

With this in mind, rather than trying to pinpoint individual residues, it is necessary to consider unique elements distinguishing functionally characterized Al-responsive and Al-insensitive ALMTs. For this purpose, we compared the amino acid sequences of all ALMT transporters functionally characterized to date. These were divided into two sub-groups containing: (i) the Al-responsive channels TaALMT1, AtALMT1 and BnALMT1, as well as HvALMT1, the latter being mildly stimulated by extracellular Al (an approximately 0.4-fold increase in transport compared with the 2–3-fold increase reported for the other ALMTs upon exposure to Al), and (ii) the Al-insensitive channels ZmALMT1 and ZmALMT2 from *Zea mays*, AtALMT6, AtALMT9 and AtALMT12 from *Arabidopsis thaliana* and GmALMT1 from *Glycine max*. It is worth noting that ZmALMT1 was assumed to be Al-insensitive given its very low level of Al sensitivity (an approximately 0.1-fold increase in transport activity upon exposure to Al). We particularly focused on structural/functional analysis of the negatively charged residues in TaALMT1 as described above. Among all of the negatively charged residues, only those in the motif [D,E]-[H,K,R]-x-[K,R]-[D,E]-x-x-x-[D,E] within the N-terminus prior to TM1–6 appear to be associated with Al responsiveness (Figure 6a). A screen of the available 403 ALMT sequences identified this motif in 19 of

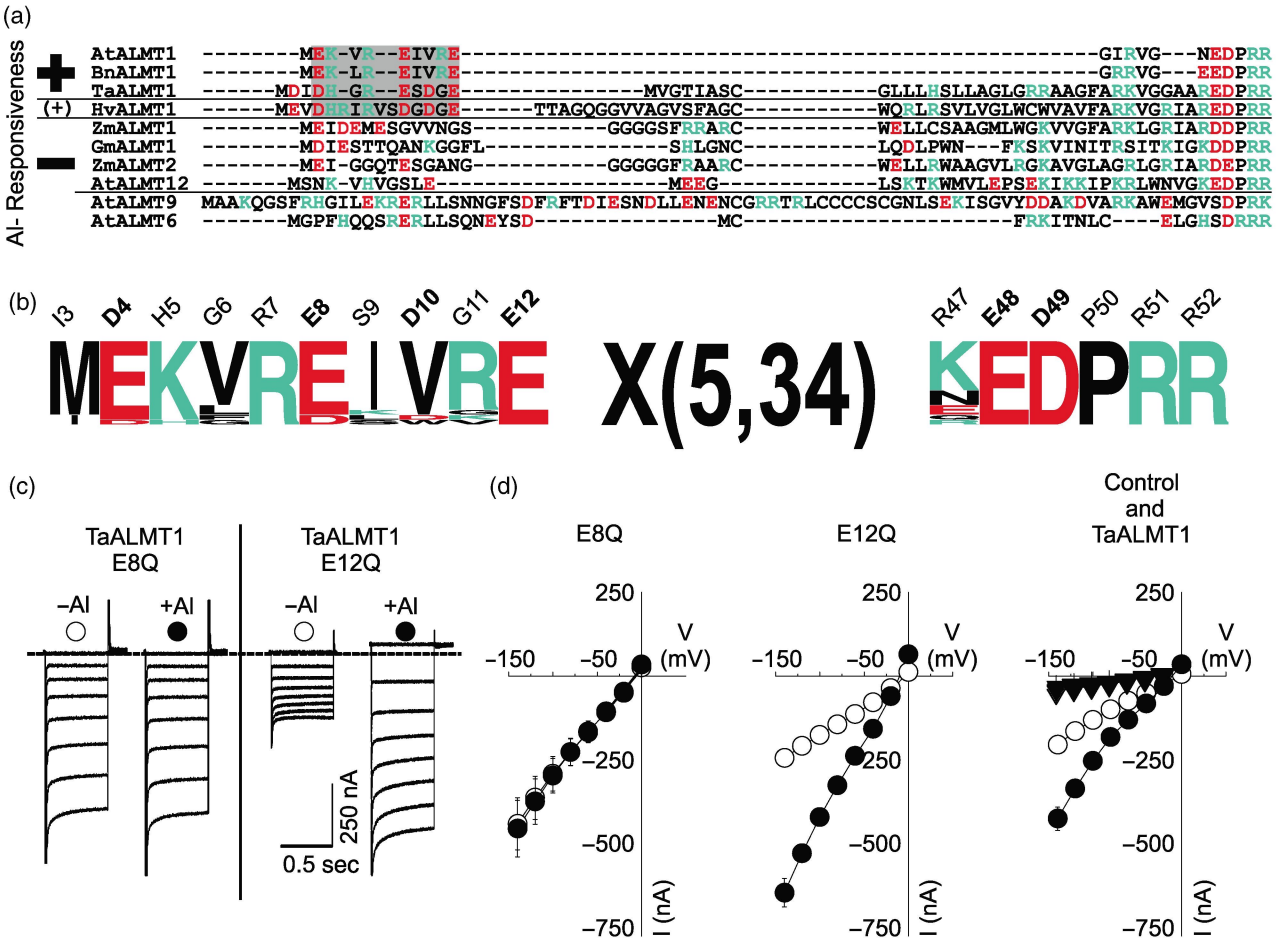

Figure 6. Putative motif determining the Al responsiveness of TaALMT1.

(a) Alignment of the N-terminal regions upstream of the first transmembrane domain of the Al-responsive (+) channels TaALMT1, AtALMT1 and BnALMT1, the mildly Al-responsive channel HvALMT1, and the Al-insensitive (–) channels ZmALMT1, ZmALMT2, GmALMT1, AtALMT12, AtALMT9 and AtALMT6, with the latter two being localized to the vacuolar membrane. The [D,E]-[H,K,R]-x-[K,R]-[D,E]-x-x-x-[D,E] motif that is unique to Al-responsive channels is indicated by a gray box.

(b) Screening of 403 ALMT sequences resulted in 17 hits in the N-terminal region of 17 channels. The sequence logo illustrates the conservation of the motif and its surrounding environment in this channel subset. The 400 ALMT sequences identified previously in higher plants (Dreyer *et al.*, 2012) together with the sequences for BnALMT1, TaALMT1 and HvALMT1 were scanned for the presence of the [K,R,H]-x-[R,K]-[E,D]-x-x-x-[E,D] motif using the ScanProsite tool (http://prosite.expasy.org/scanprosite/).

(c) Sample current traces recorded in cells expressing constructs with two neutralizations of acidic residues (E8Q and E12Q) in the putative motif determining Al responsiveness. Holding potentials ranged from −140 to 0 mV (+20 mV steps) using the voltage protocol described in Experimental Procedures. Recordings were performed in ND96 (pH 4.5) with or without Al^{3+} as indicated above each set of traces. The solid horizontal line represents the zero current level. Current traces from control cells (i.e. not injected with cRNA) and full-length TaALMT1 are shown in Figure 1(b).

(d) Mean current–voltage (*I*/*V*) curves constructed from steady-state current recordings such as those shown in (c). Symbols for each construct and ionic condition tested correspond to the symbols above the representative traces shown in (c). Mean current–voltage (*I*/*V*) curves recorded in control oocytes (triangles) and oocytes expressing the full-length unmodified TaALMT1 (circles, representing with or without Al) for this batch of experiments are shown in the far-right graph for reference.

them (Table 3). Based on the amino acid frequencies, only three or four hits were expected, indicating a significant accumulation of this motif. Interestingly, the motif was over-represented exclusively in the N-terminal regions of ALMTs from clade 1, to which the three known Al-responsive ALMTs and the less responsive HvALMT1 belong (Figure 6b and Table 3). Residue substitutions in this motif or in the immediately surrounding residues resulted in major effects, ranging from loss of Al responsiveness (e.g. E8Q and D10N; Figures 6c,d and 5c, respectively), a reduction of Al responsiveness (e.g. D2N and D4N; Figure 5c), and even Al hyper-responsiveness (E12Q; Figure 6c,d). Likewise, indels in this motif region, such as those present in HvALMT1, result in transporters with moderate/minor Al responsiveness, suggesting that, in nature, the Al-activation trait is unlikely to be a discrete functional characteristic, but rather is represented by a continuum of Al responsiveness. Our data indicate that this identified motif plays a major role in the Al-binding/gating modification processes underlying Al responsiveness. It remains unclear

Table 3 Conservation of the N-terminal Al-responsive motif throughout all ALMT clades

Clade	Number of sequences in dataset	Number of sequences with hits	Statistically expected hits in the dataset	Number of sequences with hits in the N-terminus
1	130	17	0.89	17 (100%)
2	101	2	1.12	0
3	85	0	0.76	0
4	58	0	0.38	0
5	22	0	0.17	0
Pp	5	0	0.07	0
Sm	2	0	0.00	0
Total	403	19	3.37	17

Screening of 403 ALMTs sequences for the [D,E]-[H,K,R]-x-[K,R]-[D,E]-x-x-x-[D,E] motif resulted in 19 hits, including 17 hits in regions before the first transmembrane regions. The ALMTs were separated into seven clades; clades 1–5 contain ALMTs from angiosperms, clade Pp contains ALMTs from *Physcomitrella patens*, and clade Sm contains ALMTs from *Seleginella moellendorffii* (Dreyer *et al.*, 2012).

how the Al^{3+} interactions with these and other regions of the TaALMT1 protein are coordinated to ultimately modify the gating (closed or opened conformation). Plausible scenarios involve exposure to Al^{3+} resulting in binding/bridging or disruption of interactions among several protein domains/regions (potentially the N- and C-domain), which, in turn, causes structural and conformational changes that lead to alterations in gating and consequently in transport activity. Further analysis of this N-terminal region, as well as a better structural and topological understanding of the ALMT family, is required to verify the putative role of this domain as well as some of the single residues identified in this study.

CONCLUSIONS

Although the N-domain of TaALMT1, which is predicted to contain the six transmembrane regions constituting the conductive pathway, mediates ion transport in the absence of the C-domain, both domains are required for Al^{3+}-dependent enhancement of transport. Our study highlights the importance of integrating structure–function studies with a comprehensive phylogenetic analysis, as significant functional changes may result from alterations of family-wide structural integrity, rather than modification of residues specifically associated with a particular functional characteristic. Using such an approach, we have identified a motif in the N-terminus that is potentially associated with the Al-responsive phenotype of TaALMT1. Future structural and functional studies aimed at detailed characterization of the residues present in this motif should provide a mechanistic understanding of the processes involved in the Al-mediated enhancement of TaALMT1 transport activity.

EXPERIMENTAL PROCEDURES

Functional analysis of the complementary RNA (cRNA) encoding the full-length TaALMT1, as well as truncated and single-residue mutation variants of TaALMT1, was performed by electrophysiological analysis using conventional two-electrode voltage clamp of *Xenopus* oocytes expressing these constructs. cRNA was synthesized from 1 μg *Bam*HI-linearized plasmid DNA template using an mMessage mMachine T7 *in vitro* transcription kit (Ambion, http://www.lifetechnologies.com/us/en/home/brands/ambion.html) according to the manufacturer's instructions. All constructs were generated by PCR amplification using Phusion Hot Start DNA polymerase (Finnzymes, http://www.thermoscientificbio.com/finnzymes//) with 5′ *Bgl*II and 3′ *Spe*I adaptors flanking the open reading frame (ORF), allowing their cloning between the 5′ and 3′ untranslated regions of a *Xenopus* β-globin gene present in the T7TS vector (Piñeros *et al.*, 2008b). Carboxylic end truncations were performed by introducing a premature stop codon. Single point mutations resulting in neutralization of Asp (D) to Asn (N) or Glu (E) to Gln (Q), or single point mutations of the Phe (F) or Trp (W) neutral residues to Ala (A), were generated using an overlap extension PCR method, involving two rounds of PCR (Ho *et al.*, 1989). In the first round, two separate PCR fragments (N and C halves) were generated using primers that introduced the mutated codon on both the sense and antisense strands, as well as providing an overlapping region among the fragments. These fragments were combined and used as templates for a second round of PCR using TaALMT1 5′ N- and 3′ C-terminal primers containing the *Bgl*II and *Spe*I adaptors suitable for cloning into the T7TS vector. GFP::ORF chimeras were constructed by first cloning the EGFP gene into the T7TS vector, and then subcloning the ORF of interest in-frame into the *Spe*I site of the T7TS vector. All constructs were fully sequenced and checked for sequence accuracy.

Electrophysiological recordings

Harvesting of *Xenopus laevis* oocytes and cRNA injections were performed as described previously (Piñeros *et al.*, 2008b). Oocytes were injected with 50 nl cRNA (600 ng μl^{-1}) of the desired construct. Electrophysiological recordings were performed after 3–4 days of incubations at 18°C. Whole-cell currents were recorded using a GeneClamp 500 amplifier (Axon Instruments, http://www.moleculardevices.com/) using the two-electrode voltage-clamp technique as described previously (Piñeros *et al.*, 2008b). All recordings were performed in cells pre-loaded with malate, which was achieved by micro-injecting 50 nl of 100 mM sodium malate solution 3–4 h prior to the electrophysiological recordings. Recordings were performed under constant perfusion in ND96 solution containing 96 mM NaCl, 1 mM KCl, 1.8 mM $CaCl_2$ and 0.1 mM $LaCl_3$, with or without 0.1 $AlCl_3$ (pH 4.5). Unless otherwise specified, all currents were elicited by voltage pulses stepped between -140 and 0 mV in 20 mV intervals with a 6 sec rest at 0 mV between each voltage pulse. Steady-state current–voltage (*I*/*V*) relationships were constructed by measuring the current amplitude at the end of the test pulse. Values shown are means ± SEM of at least ten independent measurements from oocytes from at least two donor frogs. The changes in transport activity are given relative to that for full-length unmodified TaALMT1, which was recorded in each batch of recordings as an internal control.

Cellular localization of EGFP and YFP chimeras

Yellow fluorescent protein (YFP) chimeras generated by sub-cloning the construct of interest into the expression vector pSAT-1413 (Citovsky *et al.*, 2006) were transiently expressed in Arabidopsis

mesophyll protoplasts using the polyethylene glycol method as described previously (Yoo *et al.*, 2007; Ligaba *et al.*, 2012). *Xenopus laevis* oocytes expressing EGFP::chimeras were fixed with 4% paraformaldehyde and sectioned. Confocal imaging was performed using a TCS SP5 confocal laser scanning microscope (Leica, http://www.leica-microsystems.com) at excitation and emission wavelengths of 514 and 525–550 nm, respectively, for the EYFP-tagged constructs, and 488 and 500–540 nm, respectively, for the EGFP-tagged constructs.

Phylogenetic analysis

The list of genes used in the phylogenetic analysis is given in Dreyer *et al.* (2012: Supporting Information, Data Sheet 3.XLSX).

ACKNOWLEDGEMENTS

The authors would like to thank Xiaomin Jia and Eric Craft for technical support. This project was supported by National Research Initiative Competitive Grant 2007-35100-18436 from the US Department of Agriculture Cooperative State Research, Education and Extension awarded to L.V.K and M.P. I.D. was supported by grants from the Spanish Ministerio de Economía y Competitividad (BFU2011-28815) and a Marie-Curie Career Integration grant (FP7-PEOPLE-2011-CIG No. 303674 – Regopoc).

REFERENCES

Citovsky, V., Lee, L.Y., Vyas, S., Glick, E., Chen, M.H., Vainstein, A., Gafni, Y., Gelvin, S.B. and Tzfira, T. (2006) Subcellular localization of interacting proteins by bimolecular fluorescence complementation *in planta*. *J. Mol. Biol.* **362**, 1120–1131.

De Angeli, A., Zhang, J., Meyer, S. and Martinoia, E. (2013) AtALMT9 is a malate-activated vacuolar chloride channel required for stomatal opening in Arabidopsis. *Nat. Commun.* **4**, 1804.

Delhaize, E., Ryan, P.R., Hebb, D.M., Yamamoto, Y., Sasaki, T. and Matsumoto, H. (2004) Engineering high-level aluminum tolerance in barley with the ALMT1 gene. *Proc. Natl Acad. Sci. USA*, **101**, 15249–15254.

Dreyer, I., Gomez-Porras, J.L., Riaño Pachon, D.M., Hedrich, R. and Geiger, D. (2012) Molecular evolution of slow and quick anion channels (SLACs and QUACs/ALMTs). *Front. Plant Sci.* **3**, 263.

Furuichi, T., Sasaki, T., Tsuchiya, Y., Ryan, P.R., Delhaize, E. and Yamamoto, Y. (2010) Extracellular hydrophilic carboxylic-terminal domain regulates the activity of TaALMT1, the aluminum-activated malate transport protein of wheat. *Plant J.* **64**, 47–55.

Gonzalez, W., Riedelsberger, J., Morales-Navarro, S.E., Caballero, J., Alzate-Morales, J.H., González-Nilo, F.D. and Dreyer, I. (2012) The pH-sensor of the plant K^+ uptake channel KAT1 is built of a sensory cloud rather than of single key amino acids. *Biochem. J.* **442**, 57–63.

Gordon, S.E., Varnum, M.D. and Zagotta, W.N. (1997) Direct interaction between amino- and carboxyl-terminal domains of cyclic nucleotide-gated channels. *Neuron*, **19**, 431–441.

Gruber, B.D., Ryan, P.R., Richardson, A.E., Tyerman, S.D., Ramesh, S., Hebb, D.M., Howitt, S.M. and Delhaize, E. (2010) HvALMT1 from barley is involved in the transport of organic anions. *J. Exp. Bot.* **61**, 1455–1467.

Ho, H.N., Hunt, H.D., Morton, R.M., Pullen, K.K. and Pease, L.R. (1989) Site-directed mutagenesis by overlap extension using the polymerase chain reaction. *Gene*, **77**, 51–59.

Hoekenga, O.A., Maron, L.G., Cançado, G.M.A. *et al.* (2006) AtALMT1 (At1 g08430) is a novel, essential factor for aluminum tolerance in Arabidopsis thaliana and encodes an aluminum-activated malate transporter. *Proc. Natl Acad. Sci. USA*, **103**, 9734–9743.

Huang, C.F., Yamaji, N., Mitani, N., Yano, M., Nagamura, Y. and Ma, J.F. (2009) A bacterial-type ABC transporter is involved in aluminum tolerance in rice. *Plant Cell*, **21**, 655–667.

Huang, C.F., Yamaji, N., Chen, Z. and Ma, J.F. (2012) A tonoplast-localized half-size ABC transporter is required for internal detoxification of aluminum in rice. *Plant J.* **69**, 857–867.

Kochian, L.V., Hoekenga, O.A. and Pineros, M.A. (2004) How do crop plants tolerate acid soils? Mechanisms of aluminum tolerance and phosphorous efficiency. *Annu. Rev. Plant Biol.* **55**, 459–493.

Kovermann, P., Meyer, S., Hörtensteiner, S., Picco, C., Scholz-Starke, J., Ravera, S., Lee, Y. and Martinoia, E. (2007) The Arabidopsis vacuolar malate channel is a member of the ALMT family. *Plant J.* **52**, 1169–1180.

Larsen, P.B., Geisler, M.J.B., Jones, C.A., Williams, K.M. and Cancel, J.D. (2005) ALS3 encodes a phloem-localized ABC transporter-like protein that is required for aluminum tolerance in Arabidopsis. *Plant J.* **41**, 353–363.

Larsen, P.B., Cancel, J., Rounds, M. and Ochoa, V. (2007) *Arabidopsis ALS1* encodes a root tip and stele localized half type ABC transporter required for root growth in an aluminum toxic environment. *Planta*, **225**, 1447–1458.

Liang, C., Piñeros, M.A., Tian, J., Yao, Z., Sun, L., Liu, J., Shaff, J., Coluccio, A., Kochian, L.V. and Liao, H. (2013) Low pH, aluminum and phosphorus coordinately regulate malate exudation through GmALMT1 to improve soybean adaptation to acid soils. *Plant Physiol.* **161**, 1347–1361.

Ligaba, A., Katsuhara, M., Ryan, P.R., Shibasaka, M. and Matsumoto, H. (2006) The *BnALMT1* and *BnALMT2* genes from rape encode aluminum-activated malate transporters that enhance the aluminum resistance of plant cells. *Plant Physiol.* **142**, 1294–1303.

Ligaba, A., Kochian, L. and Piñeros, M. (2009) Phosphorylation at S384 regulates the activity of the TaALMT1 malate transporter that underlies aluminum resistance in wheat. *Plant J.* **60**, 411–423.

Ligaba, L., Maron, L., Shaff, J., Kochian, L. and Piñeros, M. (2012) Maize ZmALMT2 is a root anion transporter that mediates constitutive root malate efflux. *Plant, Cell Environ.* **35**, 1185–1200.

Ma, J.F., Ryan, P.R. and Delhaize, E. (2001) Aluminium tolerance in plants and the complexing role of organic acids. *Trends Plant Sci.* **6**, 273–278.

Meyer, S., Mumm, P., Imes, D., Endler, A., Weder, B., Al-Rasheid, K.A.S., Geiger, D., Marten, I., Martionia, E. and Hedrich, R. (2010a) AtALMT12 represents an R-type anion channel required for stomatal movement in *Arabidopsis* guard cells. *Plant J.* **63**, 1054–1062.

Meyer, S., De Angeli, A., Fernie, A.R. and Martinoia, E. (2010b) Intra- and extra-cellular excretion of carboxylates. *Trends Plant Sci.* **15**, 40–47.

Meyer, S., Scholz-Starke, J., De Angeli, A., Kovermann, P., Burla, B., Gambale, F. and Martinoia, E. (2011) Malate transport by the vacuolar AtALMT6 channel in guard cells is subject to multiple regulation. *Plant J.* **67**, 247–257.

Motoda, H., Sasaki, T., Kano, Y., Ryan, P.R., Delhaize, E., Matsumoto, H. and Yamamoto, Y. (2007) The membrane topology of ALMT1, an aluminum-activated malate transport protein in wheat (*Triticum aestivum*). *Plant Signal. Behav.* **2**, 467–472.

Mumm, P., Imes, D., Martinoia, E., Al-Rasheid, K.A.S., Geiger, D., Marten, I. and Hedrich, R. (2013) C-terminus mediated voltage gating of Arabidopsis guard cell anion channel QUAC1. *Mol. Plant*, **6**, 1550–1563.

Negishi, T., Oshima, K., Hattori, M., Kanai, M., Mano, S., Nishimura, M. and Yoshida, K. (2012) Tonoplast- and plasma membrane-localized aquaporin-family transporters in blue hydrangea sepals of aluminum hyperaccumulating plant. *PLoS One*, **7**, e43189.

Negishi, T., Oshima, K., Hattori, M. and Yoshida, K. (2013) Plasma membrane-localized Al-transporter from blue hydrangea sepals is a member of the anion permease family. *Genes Cells*, **18**, 341–352.

Pereira, J., Zhou, G., Delhaize, E., Richardson, T. and Ryan, P.R. (2010) Engineering greater aluminium resistance in wheat by over-expressing *TaALMT1*. *Ann. Bot.* **106**, 205–214.

Piñeros, M. A. and Kochian, L. V. (2001) A Patch-Clamp Study on the Physiology of Aluminum Toxicity and Aluminum Tolerance in Maize. Identification and Characterization of Al3+-Induced Anion Channels. *Plant Physiol.*, **125**, 292–305.

Piñeros, M.A., Cancado, G.M.A., Maron, L.G., Lyi, S.M., Menossi, M. and Kochian, L.V. (2008a) Not all ALMT1-type transporters mediate aluminum-activated organic acid responses: the case of ZmALMT1, an anion-selective transporter. *Plant J.* **53**, 352–367.

Piñeros, M.A., Cancado, G.M.A. and Kochian, L.V. (2008b) Novel properties of the wheat aluminum tolerance organic acid transporter (TaALMT1) revealed by electrophysiological characterization in *Xenopus* oocytes: functional and structural implications. *Plant Physiol.* **147**, 2131–2146.

Piskorowski, R. and Aldrich, R.W. (2002) Calcium activation of BKCa potassium channels lacking the calcium bowl and RCK domains. *Nature*, **420**, 499–503.

Ryan, P. R., Skerrett, M., Findlay, G. P., Delhaize, E. and Tyerman, S. D. (1997) Aluminum activates an anion channel in the apical cells of wheat roots. *Proc. Natl. Acad. Sci. USA*, **94**, 6547–6552.

Ryan, P.R., Tyerman, S.D., Sasaki, T., Furuichi, T., Yamamoto, Y., Zhang, W.H. and Delhaize, E. (2011) The identification of aluminium-resistance genes provides opportunities for enhancing crop production on acid soils. *J. Exp. Bot.* **62**, 9–20.

Sasaki, T., Yamamoto, Y., Ezaki, B., Katsuhara, M., Ahn, S.J., Ryan, P.R., Delhaize, E. and Matsumoto, H. (2004) A wheat gene encoding an aluminum-activated malate transporter. *Plant J.* **37**, 645–653.

von Uexkull, H.R. and Mutert, E. (1995) Global extent, development and economic impact of acid soils. In *Plant–Soil Interactions at Low pH: Principles and Management* (Date, R.A., Grundon, N.J., Raymet, G.E. and Probert, M.E., eds). Dordrecht, The Netherlands: Kluwer Academic, pp. 5–19.

Varnum, M.D. and Zagotta, W.N. (1997) Interdomain interactions underlying activation of cyclic nucleotide-gated channels. *Science*, **278**, 110–133.

Xia, J., Yamaji, N., Kasai, T. and Ma, J.F. (2010) Plasma membrane-localized transporter for aluminum in rice. *Proc. Natl Acad. Sci. USA*, **107**, 18381–18385.

Yoo, S.D., Cho, Y.H. and Sheen, J. (2007) Arabidopsis mesophyll protoplasts: a versatile cell system for transient gene expression analysis. *Nat. Protoc.* **2**, 1565–1572.

Yamaguchi, M., Sasaki, T., Sivaguru, M., Yamamoto, Y., Osawa, H., Ahn, S. J. and Matsumoto, H. (2005) Evidence for the plasma membrane localization of Al-activated malate transporter (ALMT1). *Plant Cell Physiol.* **46**, 812–816.

Zhang, W.H., Ryan, P.R., Sasaki, T., Yamamoto, Y., Sullivan, W. and Tyerman, S.D. (2008) Characterization of the TaALMT1 protein as an Al^{3+}-activated anion channel in transformed tobacco (*Nicotiana tabaccum* L.) cells. *Plant Cell Physiol.* **49**, 1316–1330.